Inorganic Chemistry

Article

pubs.acs.org/IC

Spontaneous Magnetization in Homometallic μ_6-Oxalate Coordination Polymers

M. Nieves Corella-Ochoa,[†] Jordi Benet-Buchholz,[†] Marta Martínez-Belmonte,[†] and José Ramón Galán-Mascarós*[,†,‡]

[†]Institute of Chemical Research of Catalonia (ICIQ), Avenida Països Catalans 16, 43007 Tarragona, Spain

[‡]Catalan Institute of Research and Advanced Studies, Passeig Lluïs Companys 23, 08010 Barcelona, Spain

Supporting Information

ABSTRACT: The reaction of 1,2,4-triazole and NaF with M(ox) (M = transition-metal dication; ox = oxalate dianion) under hydrothermal conditions has led to the isolation of a variety of hybrid organic−inorganic coordination polymers. Four structurally different 3D networks were obtained, depending on the transition metal, with stoichiometry $[M_2(H_2O)(\mu_2\text{-ox})][M_2(\mu_3\text{-trz})_6]$ [M = Fe (**1**), Co (**2**), Ni (**3**)], $[Zn_2(H_2O)(\mu_3\text{-trz})_2(\mu_2\text{-ox})]$ (**4**), $[Mn_3(\mu_3\text{-trz})_2(\mu_6\text{-ox})(\mu_3\text{-F})_2]$ (**5**), and $[Fe_3(\mu_3\text{-trz})_2(\mu_6\text{-ox})(\mu_2\text{-F})_2]$ (**6**). In all cases, the magnetic behavior is dominated by antiferromagnetic exchange interactions between paramagnetic centers. Remarkably, **5** and **6** present a novel magnetic connectivity around the oxalate anion: a μ_6-bridging mode. This magnetic geometry promotes multiple triangular arrangements among antiferromagnetically coupled spin carriers, resulting in a complex magnetic network because of the presence of competing interactions. These materials exhibit spontaneous magnetization below 9 and 66 K, respectively.

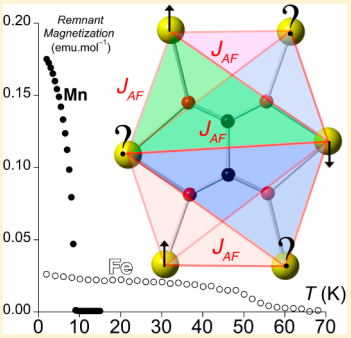

INTRODUCTION

Over the past decades, organic−inorganic hybrid coordination polymers have occupied a prominent position in the field of materials science because of their wide range of technological applications.[1−5] The design tools are well established and involve the use of connectors (inorganic units, metal complexes, etc.) and linkers (organic molecules) as the main building units. Both parts play a crucial role in the functionality of the final structure. In the field of magnetic materials, molecule-based magnets[6] have successfully reached features usually associated with classic inorganic solids, such as high ordering temperatures[7−10] or large magnetic hysteresis.[11,12] These unique materials possess, at the same time, properties typically associated with molecules: light-weight, transparent, easily processable, etc.

The design of molecule-based magnets requires the use of linkers able to promote strong superexchange interactions when high-temperature magnetic phenomena are desired. This means that short bridges between spin carriers are mandatory. Single-atom bridges, such as oxo or fluoride, promote very strong coupling.[13] However, it is synthetically difficult to incorporate such highly electronegative connectors maintaining a molecular character because they favor the formation of ionic solid-state compounds.

The most successful ligands in the search for molecule-based magnets have been short (two or three atoms) bridges with an efficient π pathway such as cyanide,[14−18] carboxylate,[19] oxalate,[20−25] azide,[26−29] or dicyanamide.[14,30−34] These organic ligands promote ferromagnetic (FM) or antiferromagnetic (AF) exchange interactions depending on their connecting modes. FM interactions are typically weak, whereas AF interactions can be very strong, resulting in high-temperature magnetic phenomena. However, AF coupling typically stabilizes a nonmagnetic ground state in homometallic compounds because of the alternating orientation of identical spins. To take advantage of these strong AF interactions, heterometallic compounds or organic radicals linkers[35] have been used to yield high-temperature ferrimagnets. Homospin systems, where the AF interactions are maximized because of the perfect energy matching between atomic orbitals, need the appearance of spin canting between antiparalleled magnetic moments to yield weak ferromagnets.[36−38] Spin canting depends on small deviations from perfect alignment between local magnetic moments due to geometrical or electronic anisotropy.[39]

The electronic origin for the canted alignment of spins can arise from single-ion anisotropy and/or antisymmetric spin−spin coupling (termed Dzyaloshinskii−Moriya interaction). Geometrical anisotropy appears when the crystal lattice is incompatible with dominant AF interactions. This is the case, for example, in a triangular array of antiferromagnetically coupled metal centers. This geometry promotes competing AF interactions[40] and stabilization of a magnetic ground state.[41,42] The appearance of spontaneous magnetization in strongly antiferromagnetically coupled homospin systems keeps attracting interest as a plausible strategy to reach high ordering temperatures.[43,44] The best examples have appeared in oxo-centered triangular arrays.[45]

The multidentate oxalate (ox) ligand is the shortest organic ligand with more coordination modes able to induce triangular

Received: December 21, 2014
Published: May 7, 2015

DOI: 10.1021/ic503032g
Inorg. Chem. 2015, 54, 4678−4687

arrangements when it connects more than two centers (Figure 1). Although, the main connecting mode with transition metals

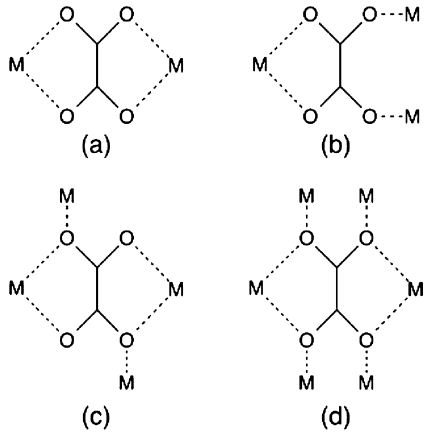

Figure 1. Bridging coordination modes of an oxalate anion with transition-metal cations (M): (a) μ-bridging mode; (b) μ_3-bridging mode; (c) μ_4-bridging mode; (d) μ_6-bridging mode, unprecedented for six paramagnetic transition-metal centers.

is μ_2-bis-chelating (Figure 1a), with higher connectivity being rare.[23] The most promising mode for the development of magnetic materials is μ_6 (Figure 1d) because it should promote competing interactions arising from the multiple triangular arrangements, but to date, it has only been reported with diamagnetic alkali-metal ions.

Here we report multicomponent reactions by combining oxalate, 1,2,4-trizolate, and fluoride ligands with divalent metal centers. We have been able to isolate six novel compounds under hydrothermal conditions, belonging to four structural motifs: $[M_2(H_2O)(\mu_2\text{-ox})][M_2(\mu_3\text{-trz})_6]$ [M = Fe (**1**), Co (**2**), Ni (**3**)], $[Zn_2(H_2O)(\mu_3\text{-trz})_2(\mu_2\text{-ox})]$ (**4**), $[Mn_3(\mu_3\text{-trz})_2(\mu_6\text{-ox})(\mu_3\text{-F})_2]$ (**5**), and $[Fe_3(\mu_3\text{-trz})_2(\mu_6\text{-ox})(\mu_2\text{-F})_2]$ (**6**). These materials represent a new family of oxalate-based coordination polymers with unprecedented architectures. Remarkably, the elusive μ_6-oxalate bridging mode has been found in compounds **5** and **6**, which induces competing interactions and the appearance of spontaneous magnetization.

EXPERIMENTAL SECTION

All reagents and chemicals were supplied by Sigma-Aldrich Chemical Co. Ltd. and Acros Organics. Unless stated otherwise, the materials were used without further purification. Elemental analyses (C, H, N, and F) were carried out by iQAC Servei de Microanàlisis (CSIC, Barcelona, Spain). Fourier transform infrared (FT-IR) spectra were collected in transmission mode using a Bruker Optics FT-IR Alpha spectrometer in the 4000−400 cm^{-1} range. Thermogravimetric analyses (TGA) were performed with a TGA/SDTA851 Mettler Toledo analyzer under a nitrogen flow at a heating rate of 10 °C min^{-1}. Powder X-ray diffraction (PXRD) data were collected on a D8 Advance series $2\theta/\theta$ powder diffractometer at room temperature. Magnetic susceptibility measurements between 2 and 300 K were carried out in a Quantum Design MPMS-XL SQUID magnetometer

Table 1. Crystallographic Data and Main Refinement Parameters for Compounds 1 and 4−6

compound	**1**	**4**	**5**	**6**
formula	$C_{14}H_{20}Fe_4N_{18}O_8$	$C_6H_{12}N_6O_8Zn_2$	$C_6H_4F_2Mn_3N_6O_4$	$C_{12}H_8F_4Fe_6N_{12}O_8$
MW	791.88	426.96	426.97	859.40
T (K)		100(2)		
wavelength (Å)		0.71073		
cryst syst		monoclinic		
space group	$C2$	$P2_1/c$	$P2_1/n$	$C2/c$
a (Å)	15.653(3)	7.4835(16)	7.7577(3)	7.5869(7)
b (Å)	10.750(2)	8.8171(19)	7.2598(3)	12.6052(11)
c (Å)	7.2868(14)	10.058(2)	9.8914(4)	11.5603(10)
β (deg)	90.361(6)	100.450(6)	93.941(2)	101.775(3)
V (Å^3)	1226.2(4)	652.7(2)	555.76(4)	1082.30(17)
Z	8	4	2	2
D_{calc} (g cm^{-3})	2.145	2.173	2.551	2.637
abs coeff (mm^{-1})	2.405	3.731	3.412	4.026
F(000)	796	428	414	840
size (mm^3)	0.15 × 0.12 × 0.08	0.01 × 0.01 × 0.002	0.05 × 0.01 × 0.002	0.30 × 0.30 × 0.10
θ range (deg)	2.30−25.63°	2.768−33.193°	3.455−36.366°	3.184−36.304°
index ranges	$-17 \le h \le 18$	$-5 \le h \le 11$	$-12 \le h \le 10$	$-12 \le h \le 8$
	$-13 \le k \le 13$	$-13 \le k \le 8$	$-12 \le k \le 11$	$-20 \le k \le 20$
	$-8 \le l \le 8$	$-15 \le l \le 14$	$-16 \le l \le 16$	$-18 \le l \le 19$
reflns collected	5928	6736	10448	7583
indep reflns	2295	2315	2687	2440
R_{int}	0.0286	0.0358	0.0384	0.0315
max/min transmn	0.8309/0.7143	0.993/0.739	0.993/0.861	0.961/0.367
data/restraints/param	2295/317/183	2315/0/100	2687/0/97	2440/258/153
GOF on F^2	1.093	1.025	1.046	1.155
R1 [$I > 2\sigma(I)$]	0.0380	0.0342	0.0186	0.0320
wR2 [$I > 2\sigma(I)$]	0.0881	0.0709	0.0494	0.0845
R1 (all data)	0.0443	0.0512	0.0200	0.0333
wR2 (all data)	0.0923	0.0765	0.0504	0.0853
largest diff peak/hole (e Å^{-3})	1.174/−0.823	1.534/−0.789	0.732/−0.403	2.096/−0.823

DOI: 10.1021/ic503032g
Inorg. Chem. 2015, 54, 4678−4687

using a 1000 Oe field. Pascal's constants were used to estimate the diamagnetic corrections for the compounds. Data for compound **1** showed a paramagnetic impurity that was also corrected, accounting for 2.5% of the total signal. Zero-field-cooled (ZFC), field-cooled (FC), and remnant magnetization (RM) measurements were carried out using a 25 Oe field. Magnetization curves were collected between −7 and 7 T at 2 and 10 K.

Synthesis of $[Fe_2(H_2O)(C_2O_4)][Fe_2(C_2H_2N_3)_6]\cdot 2.5H_2O$ (1). A mixture of Fe(ox)·$2H_2O$ (0.22 g, 1.5 mmol), 1,2,4-triazole (0.42 g, 6 mmol), NaF (50 mg), and H_2O (10 mL) was heated at 180 °C for 1 week under autogenous pressure. The mixture was cooled to room temperature. Brown prism-shaped crystals from **1**, suitable for X-ray structure analysis, were obtained. Yield: 165.1 mg, 56% (based on Fe). Elem anal. Calcd for $C_{14}H_{19}Fe_4N_{18}O_{7.5}$ (782.80): C, 21.48; H, 2.45; N, 32.21. Found: C, 21.25; H, 1.91; N, 31.93. FT-IR (cm^{-1}): 1637 s, 1488 s, 1281 s, 1145 s, 986 s, 665 s, 620 s.

Synthesis of $[Co_2(H_2O)(C_2O_4)][Co_2(C_2H_2N_3)_6]\cdot 4H_2O$ (2). A mixture of Co(ox)·$2H_2O$ (0.1 g, 0.55 mmol), 1,2,4-triazole (0.1 g, 1.45 mmol), NaF (50 mg), and H_2O (10 mL) was heated at 180 °C for 1 week under autogenous pressure. The mixture was cooled to room temperature. A pink solid of **2** was formed. Yield: 74 mg, 65% (based on Co). Elem anal. Calcd for $C_{14}H_{22}Co_4N_{18}O_9$ (822.17): C, 20.45; H, 2.7; N, 30.67. Found: C, 20.34; H, 2.45; N, 30.45. FT-IR (cm^{-1}): 1628 s, 1496 s, 1310 s, 1277 s, 1154 s, 1074 s, 993 s, 883 s, 802 s, 672 s.

Synthesis of $[Ni_2(H_2O)(C_2O_4)][Ni_2(C_2H_2N_3)_6]\cdot 4H_2O$ (3). The same procedure as that for compound **2** was followed but using Ni(ox)·$2H_2O$ instead of Co(ox)·$2H_2O$. A blue solid of **3** was formed after 1 week under autogenous pressure. Yield: 54.9 mg, 49% (based on Ni). Elem anal. Calcd for $C_{14}H_{22}Ni_4N_{18}O_9$ (821.21): C, 20.48; H, 2.7; N, 30.7. Found: C, 20.83; H, 2.36; N, 30.44. FT-IR (cm^{-1}): 1631 s, 1573 s, 1499 s, 1311 s, 1281 s, 1160 s, 1083 s, 995 s, 883 s, 674 s.

Synthesis of $[Zn_2(H_2O)(C_2H_2N_3)_2(C_2O_4)]\cdot 2H_2O$ (4). A mixture of Zn(ox)·xH_2O (50 mg, 0.26 mmol), 1,2,4-triazole (0.109 g, 1.6 mmol), NaF (50 mg), and H_2O (10 mL) was heated at 180 °C for 1 week under autogenous pressure. The mixture was cooled to room temperature. White prism-shaped crystals from **4**, suitable for X-ray structure analysis, were obtained. Yield: 30.5 mg, 29% (based on Zn). Elem anal. Calcd for $C_6H_{10}Zn_2N_6O_7$ (408.94): C, 17.62; H, 2.46; N, 20.55. Found: C, 17.88; H, 2.24; N, 20.61. FT-IR (cm^{-1}): 1622 s, 1512 s, 1354 s, 1308 s, 1212 s, 1154 s, 1079 s, 1005 s, 794 s, 662 s, 492 s.

Synthesis of $[Mn_3(C_2H_2N_3)_2(C_2O_4)F_2]$ (5). A mixture of Mn(ox)·xH_2O (0.1 g, 0.7 mmol), 1,2,4-triazole (0.97 g, 1.4 mmol), NaF (50 mg), and H_2O (10 mL) was heated at 180 °C for 3 days under autogenous pressure. The mixture was cooled to room temperature. Yellow crystals from **5**, suitable for X-ray structure analysis, were obtained. Yield: 57 mg, 57% (based on Mn). Elem anal. Calcd for $C_6H_4F_2Mn_3N_6O_4$ (426.94): C, 16.88; H, 0.94; N, 19.68. Found: C, 16.93; H, 0.94; N, 19.80. FT-IR (cm^{-1}): 1624 s, 1507 s, 1321 s, 1271 s, 1149 s, 1053 s, 993 s, 875 s, 770 s, 659 s, 513 s.

Synthesis of $[Fe_3(C_2H_2N_3)_2(C_2O_4)F_2]$ (6). A mixture of Fe(ox)·$2H_2O$ (0.1 g, 0.56 mmol), 1,2,4-triazole (0.1 g, 1.45 mmol), NaF (50 mg), and H_2O (10 mL) was heated at 180 °C for 1 week under autogenous pressure. The mixture was cooled to room temperature. **1** is the main product of this reaction, with **6** being a minor product as brown hexagonal-shaped crystals. These crystals, suitable for X-ray structure analysis, were hand-collected by the Pasteur method. All characterization was carried out with single crystals.

X-ray Crystallography. Single-crystal X-ray diffraction measurements were made at 100 K in a Bruker APEX DUO diffractometer with a Quazar MX Multilayer Optics diffractometer (Mo Kα radiation; λ = 0.71073 Å). Single-crystal X-ray diffraction measurements on **1** and **4**−**6** were made at 100 K using a Bruker-Nonius diffractometer equipped with an APEX II 4K CCD area detector, a FR591 rotating anode with Mo Kα radiation (λ = 0.71073 Å), and Montel mirrors as the monochromator. The structures were solved using the *SIR2011* program[46] and refined on F^2 using the *SHELXTL97* program.[47] Crystal data collection and refinement parameters are given in Table 1. CCDC 1033523 (**1**), 1033524 (**4**), 1033525 (**5**), and 1033526 (**6**) contain the supplementary crystallographic data for this paper. Compounds **2** and **3** are isostructural to **1**, as confirmed by the X-ray diffraction pattern from powder samples (Figure S1 in the Supporting Information, SI). Their corresponding unit cells, as estimated from the PXRD patterns, are **2** [monoclinic *C*2, a = 15.9229(8) Å, b = 11.0698(4) Å, c = 7.7171(5) Å, β = 90.488(5)°, and V = 1360.20(11) $Å^3$] and **3** [monoclinic *C*2, a = 15.7272(15) Å, b = 10.9328(9) Å, c = 7.5646(8) Å, β = 90.483(9)°, and V = 1300.64(22) $Å^3$].

RESULTS AND DISCUSSION

Synthesis. The reaction of M(ox)·$2H_2O$ (M = divalent transition metal cation; ox = oxalate dianion) and 1,2,4-triazole at 180 °C yielded four novel compounds that can be classified into two different stoichiometries: $[M_2(H_2O)(\mu\text{-ox})][M_2(\mu_3\text{-trz})_6]$ [M = Fe (**1**), Co (**2**), Ni (**3**)] and $[Zn_2(H_2O)(\mu_3\text{-trz})_2(\mu_2\text{-ox})]$ (**4**).

Single crystals suitable for X-ray diffraction analysis of **1** and **4** were obtained by adding NaF to the reaction mixture as a mineralizing agent because the presence of fluoride anions slows the crystallization dynamics. In the case of cobalt and nickel analogues, only polycrystalline powders were isolated in all tested reaction conditions.

The presence of fluoride also allowed the isolation of two additional compounds that incorporate fluoride anions into their framework: $[M_3(\mu_3\text{-trz})_2(\mu_6\text{-ox})F_2]$ [M = Mn (**5**), Fe (**6**)]. **5** is the only product that was isolated with the Mn^{2+} cation because in the absence of NaF no product was obtained. **6** is a minor product that appears when the synthesis of **1** is carried out in the presence of NaF. **6** was obtained as large and distinct single crystals, reaching a maximum 5% yield by decreasing the trz ratio in the starting materials. The large size of these single crystals allowed easy hand collection.

Structural Description. Compound **1** consists of a 3D coordination network with μ_2-oxalate and μ_3-triazolate bridges. The charge balance indicates that all Fe centers appear in the 2+ oxidation state. There are three crystallographically independent Fe positions in the structure. Fe1 is coordinated to an oxalate, a H_2O molecule, and three monodentate triazolate anions (through the N4 position). Fe2 and Fe3 are chemically equivalent, coordinated by six triazolate rings (through the N1 and N2 positions). Fe2 and Fe3 build $\{Fe(trz)_3\}$ chains running along the c axis, where the Fe^{2+} centers are connected by three triazolate bridges (Figure 2b). These 1D chains are analogous to those found in the classic triazole-based spin-transition materials.[48] The intrachain Fe−Fe distance is 3.643 Å, with Fe−N distances in the 1.89−2.06 Å range, suggesting a diamagnetic low-spin configuration. The propeller geometry of the triple trz bridge is staggered, with an almost perfect 60° torque angle between adjacent bridges, in such a way that the conformation is repeated every other bridge.

The $\{Fe(trz)_3\}$ chains are connected to each other through the triazolate N4 position, which binds to $[Fe_2(H_2O)(ox)]$ moieties via the Fe1 centers. Fe1 shows longer bonding distances (2.05−2.3 Å) to the chelated oxalate anion than to the three triazolate ligands shared with three adjacent chains and one H_2O molecule (Figure 2b). This suggests a high-spin configuration in Fe1. Each dimer connects two adjacent chains on the *ac* plane and two on the *bc* plane. The latter bridges are multiply connected to two adjacent staggered trz bridges. Single crystals included three crystallization H_2O molecules per formula unit, whereas elemental analysis and TGA in grained

DOI: 10.1021/ic503032g
Inorg. Chem. 2015, 54, 4678−4687

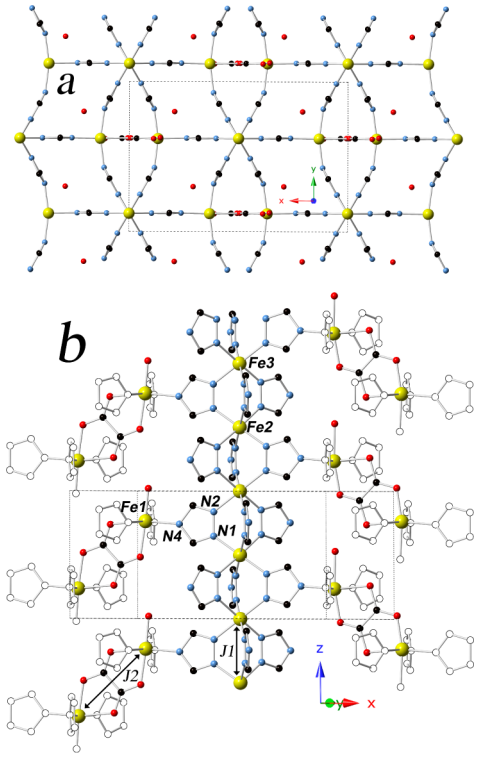

Figure 2. (a) Projection of the crystal structure of **1** on the *ab* plane. (b) Representation along the *c* axis, highlighting the triply bridged $\{Fe(trz)_3\}$ chains connected through the $[Fe_2(H_2O)(ox)]$ dimers. Color code: Fe, yellow; C, black; N, blue; O, red. H atoms omitted for clarity.

samples indicated slightly lower H_2O content (2.5 H_2O molecules per formula unit).

Compounds **2** and **3** are isostructural to **1**, as confirmed by their PXRD patterns (Figure S1 in the SI).

Compound ***4***. This polymeric network is built by only one crystallographic Zn site, coordinated by a chelating oxalate, three terminal trz units (through N1, N2, and N4, respectively), and a H_2O molecule. The structure can be described as formed by chains defined by the μ-oxalate and double μ-trz bridges along the *b* axis. The N4 position, completing the μ_3-trz connectivity, links the chains to form a 3D structure (Figure 3). Additionally, there is a second H_2O molecule making hydrogen bonds with the coordinated H_2O molecule and an oxalate anion.

Compound ***5***. There are two crystallographically independent Mn positions in this structure, in the 2+ oxidation state, according to the charge balance. One is heptacoordinated (Mn1) and one hexacoordinated (Mn2). Two trz units occupy the axial positions. One chelating and one terminal oxalate units occupy the equatorial plane, opposite to each other, completed by two F atoms. The oxalate bite shows significantly longer bonding distances (>2.4 Å) than the fluoride, terminal oxalate, and trz (in the 2.1−2.2 Å range). Mn2 shows a distorted octahedral geometry, with two F atoms in the axial positions. The equatorial positions are occupied by two monodentate oxalates and two trz ligands in *trans* configuration. The octahedron is distorted, with the axial positions significantly shorter (<2.01 Å) than the equatorial ones (>2.18 Å).

Taking into account the magnetic connectivity, the structure can be described as formed by layers (Figure 4a), perpendicular to the *ac* plane, and defined by μ_6-oxalate, μ_3-F^-, and μ_2-trz

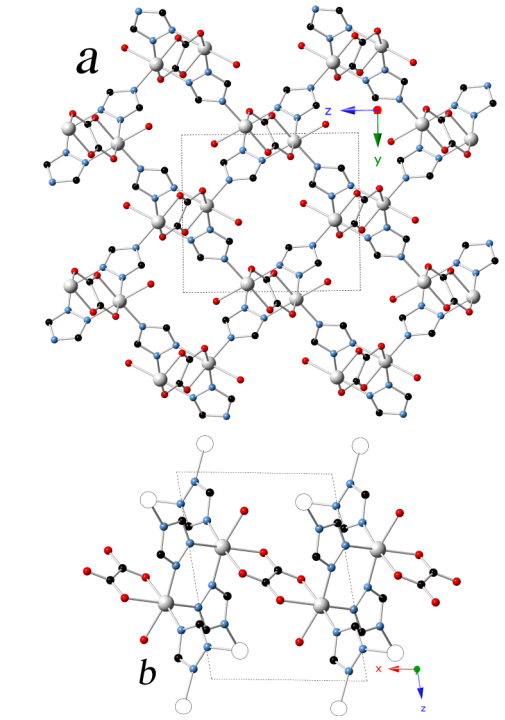

Figure 3. (a) Projection of the crystal structure of **4** on the *bc* plane. (b) Representation of the doubly bridged chains along the *b* axis. Color code: Zn, white; C, black; N, blue; O, red. H atoms omitted for clarity.

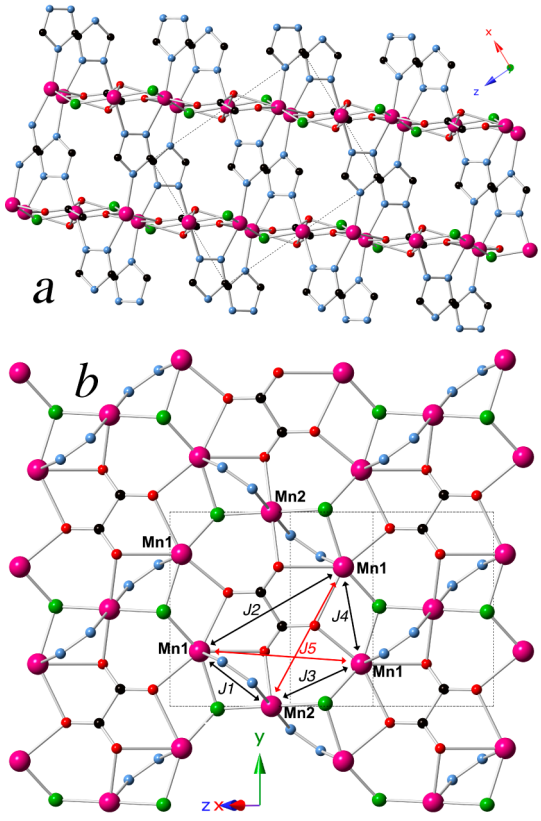

Figure 4. (a) Projection of the crystal structure of **5** on the *ac* plane. (b) Representation of the multiply bridged planes along the *b* axis, defined by the μ_6-oxalate, μ_3-F^-, and μ_2-trz bridges. Color code: Mn, pink; C, black; N, blue; O, red; F, green. H atoms omitted for clarity.

DOI: 10.1021/ic503032g
Inorg. Chem. 2015, 54, 4678−4687

bridges. The latter are above and below the plane, where the trz ligands connect layers through its third N atom. The [Mn_3F] units form a regular triangle (Mn−F = 2.283, 2.120, and 2.091 Å). The μ_6-oxalate bridge connects four Mn1 (two chelated and two terminal) and two Mn2 centers, with a longer chelating bite (Mn−O = 2.442 and 2.491 Å) and a shorter terminal bonding (Mn−O = 2.179 and 2.276 Å).

Each metal dication is surrounded by six Mn centers, in a distorted pseudohexagonal array. The bridges are a triple oxo/trz/fluoride (J_1), an oxalate (J_2), a double carboxylate/fluoride (J_3), a double oxo/fluoride (J_4), and two single carboxylates (J_5). This creates multiple triangular arrangements, with $J_1/J_2/J_5$, $J_4/J_3/J_5$, and all their equivalents by symmetry. The fluoride is also at the center of a Mn triangle (Figure 4b).

Compound ***6***. This structure is reminiscent of **5**, with identical stoichiometry. The main difference resides in both Fe^{2+} centers being hexacoordinated (pseudooctahedral) and the fluoride bridges being μ_2-F^-. Fe1 is coordinated by one chelating and one monodentate oxalates, two trz ligands (through the N1 and N4 positions), and only one fluoride. Fe2 is coordinated by two monodentate oxalate anions at the axial positions, with the equatorial positions occupied by two fluorides and two trz ligands (N1 or N2) in a *trans* configuration. In this case, the structure can be described as formed by corrugated layers parallel to the *bc* plane, defined by the μ_6-oxalate, μ_2-fluoride, and triazolate bridges, with the trz ligands bridging layers as μ_3 linkers (Figure 5).

Compared to **5**, the μ_6-oxalate connectivity shows shorter bonds, with all six Fe−O distances in the 2.1−2.3 Å range. The shortest and longest distances belong to the oxalate chelating bite. The fluoride anion is now out of the plane defined by the metal centers, bridging Fe1 and Fe2 (Fe1−F = 1.947 Å and Fe2−F = 1.980 Å). The next-nearest Fe atom appears at Fe−F = 2.760 Å, too long to be considered an effective bond. The magnetic connectivity in the plane is defined by an oxalate (J_1), two oxos (J_2 and J_5), two carboxylates (J_3), and a double trz/fluoride (J_4).

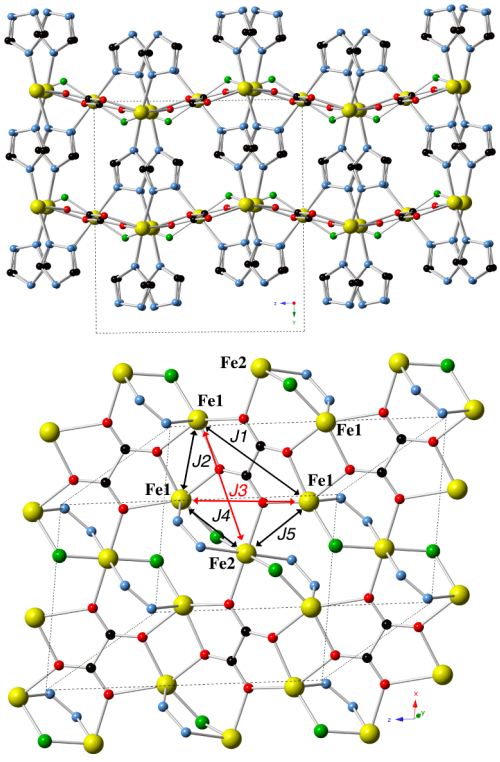

Figure 5. (a) Projection of the crystal structure of **6** on the *bc* plane. (b) Representation of the multiply bridged planes along the *a* axis, defined by the μ_6-oxalate, μ_2-F^-, and μ-trz bridges. Color code: Fe, yellow; C, black; N, blue; O, red; F, green. H atoms omitted for clarity.

Magnetic Characterization. Compounds **1**−**3** are paramagnetic at room temperature with $\chi_m T$ products of 7.60, 10.43, and 3.80 emu K mol^{-1}, respectively. This indicates high-spin M^{2+} metal centers for **2** and **3** and a mixture of low-spin Fe^{2+} (S = 0 in the chain) and high-spin Fe^{2+} (S = 2 in the dimer) for **1** (Table 2), as expected from the crystallographic data. As the temperature decreases, the $\chi_m T$ product (Figure 6) decreases, suggesting the presence of dominant AF interactions. The high-temperature regime, above 100 K, can be simulated with a Curie−Weiss law (Figure S2 in the SI), yielding negative Weiss constants following the trend $\theta(\mathbf{3}) > \theta(\mathbf{2}) > \theta(\mathbf{1})$. Below 100 K, $\chi_m T$ decreases more rapidly, approaching null values at very low temperatures. The presence of dominant AF interactions is corroborated by the appearance of a maximum in χ_m (Figure 7).

In **1**, the oxalate bridge is the only effective superexchange pathway between spin careers. Thus, the magnetic data can be modeled with an isotropic Hamiltonian for a dimer of two S centers with a J_2 coupling constant:

$$H = -J_2 S_1 S_2 \tag{1}$$

Using this Hamiltonian for S = 2, the magnetic data for compound **1** can be reproduced with a weak AF coupling (Table 2). The S = 0 low-spin configuration of the Fe centers in the chain is maintained up to 400 K. No spin transition was observed.

Because the μ_3-trz bridge should be the weakest exchange pathway compared with the triple μ_2-trz bridges along the chain and the bis-chelating oxalate bridge in the dimer, it can be considered negligible in a first approximation. Thus, we have modeled the magnetic data of **2** and **3** with an isotropic Hamiltonian result of the addition of a chain of n-spin S centers with a J_1 superexchange parameter, plus a dimer with a J_2 parameter:

$$H = -J_1 \sum_{i=1}^{n-1} S_i S_{i+1} - J_2 S_1 S_2 \tag{2}$$

Compound **2** shows strong single-ion anisotropy typical of octahedral Co^{2+} complexes. Still, we tried to model the data with the same Hamiltonian for $S = {}^3/_2$, using the analytical expression derived by Fisher for a chain:[49]

$$\chi = \frac{Ng^2\beta^2 S(S+1)}{3kT}\,\frac{1+u}{1-u} \tag{3}$$

with

$$u = \coth\left[\frac{JS(S+1)}{kT}\right] - \frac{kT}{JS(S+1)} \tag{4}$$

The best fit is surprisingly good, being obtained from an isotropic model. Although the absolute numbers for J_1 and J_2 need to be taken as a rough estimation, it is interesting to note how the AF interaction in the dimer is significantly stronger because J_2 doubles J_1.

The isotropic Hamiltonian for a chain of equally spaced isotropic S = 1 magnetic centers has an analytical expression:[50]

DOI: 10.1021/ic503032g
Inorg. Chem. 2015, 54, 4678−4687

Table 2. Magnetic Parameters for Compounds 1−3, 5, and 6

	$\chi_m T$ (emu K mol^{-1})[a]	XT_{SO}(emu K mol^{-1})	C (emu K mol^{-1})	q (K)	g	J_1 (cm^{-1})	J_2 (cm^{-1})	T_C (K)	H_{coer} (Oe)[b]
1	7.60	6.0	8.33	−28.9	2.30(1)		−5.1(2)		
2	10.43	7.5	12.45	−56.5	2.50(2)	−3.1(2)	−6.2(4)		
3	3.80	4.0	4.98	−98.4	2.20(2)	−12(1)	−16(2)		
5	11.93	13.1	13.91	−52.2	2.1[c]			9	450
6	8.93	9.0	11.74	−90.6	2.3[c]			66	

[a]300 K. [b]2 K. [c]Estimated from the Curie constant.

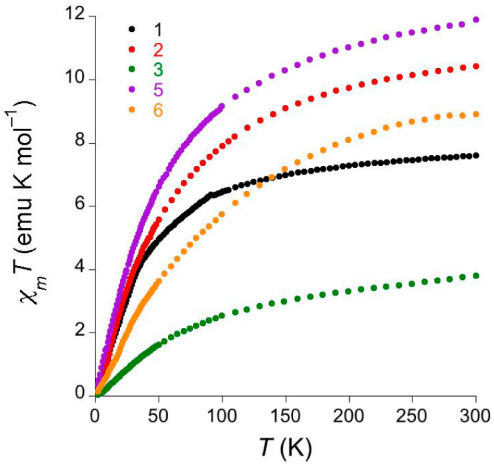

Figure 6. Thermal dependence of the $\chi_m T$ product for compounds **1**−**3**, **5**, and **6** under an applied magnetic field of 1000 Oe.

$$\chi = \frac{Ng^2\beta^2}{kT}\,\frac{2.0 + 0.0194x + 0.777x^2}{3.0 + 4.346x + 3.232x^2 + 5.834x^3}$$

$$\text{with } x = \frac{|J|}{kT} \qquad (5)$$

Using this expression for **3**, the fitting of the magnetic data yields a stronger overall AF exchange for this derivative, and $J_1 \approx 0.75J_2$ (Table 2). This is in good agreement with the exchange coupling constants found in homometallic oxalate-bridged dimers that significantly exhibited stronger coupling for Ni.[51]

Compounds **5** and **6** have a much more complex magnetic connectivity. Their magnetic data cannot be fitted to a simple model because of their layered structure with multiple and competing superexchange pathways. The room temperature $\chi_m T$ products are 11.93 and 8.93, respectively. Both numbers are lower than the expected spin-only values (Table 2). A Curie−Weiss fitting of the high-temperature data yields Curie constants in good agreement with the spin-only values (Table 2). The behavior of $\chi_m T$ under an applied field of 0.1 T is apparently very similar to that of the previous compounds (Figure 6). However, the χ_m versus T plots are quite different. In addition to the appearance of a maximum due to the dominant AF interactions, one can observe additional features that suggest the appearance of spontaneous magnetization.

In the case of **5**, χ_m shows a maximum of around 12 K and a sudden jump below 10 K (Figure 8). The ZFC and FC data show the appearance of an irreversibility (Figure 9), which suggests the onset of spontaneous magnetization. This is confirmed by the RM, which remains at zero field. RM disappears at 9.0 K, which defines the critical temperature (T_C) for this compound. Alternating-current (ac) magnetic measurements (Figure S3 in the SI) are significantly different from the direct-current (dc) data, supporting the onset of spontaneous magnetization. However, ac data are surprisingly complex. The in-phase susceptibility shows a sharp decrease below 9 K, concomitant with the appearance of a nonzero out-of-phase signal, although very weak. Even though no frequency dependence was observed. Magnetization (M) data at 2 K (Figure S4 in the SI) are essentially linear up to 7 T, when they

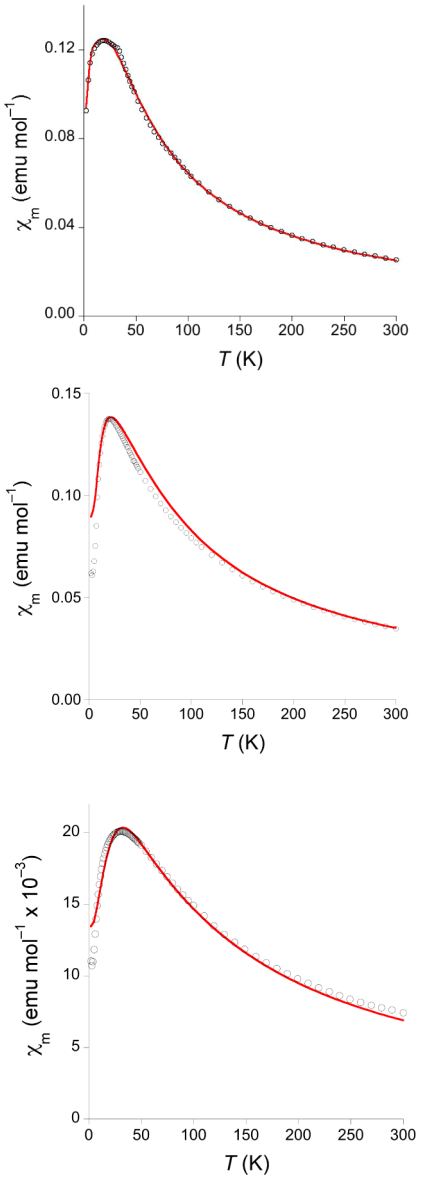

Figure 7. Thermal dependence of the magnetic susceptibility for compounds **1**−**3**, respectively, measured under an applied magnetic field of 1000 Oe. The red line shows the best fit with the model described in eq 1.

DOI: 10.1021/ic503032g
Inorg. Chem. 2015, 54, 4678−4687

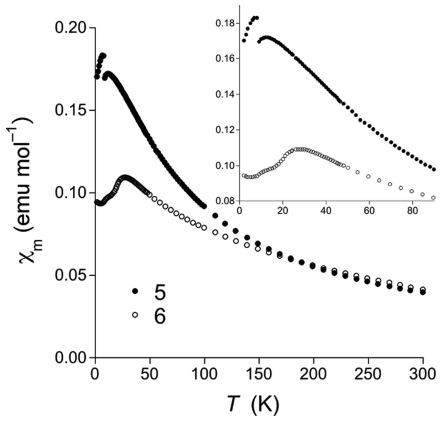

Figure 8. Thermal dependence of magnetic susceptibility for compounds **5** and **6** measured under an applied magnetic field of 1000 Oe. Inset: Detail of the low-temperature data.

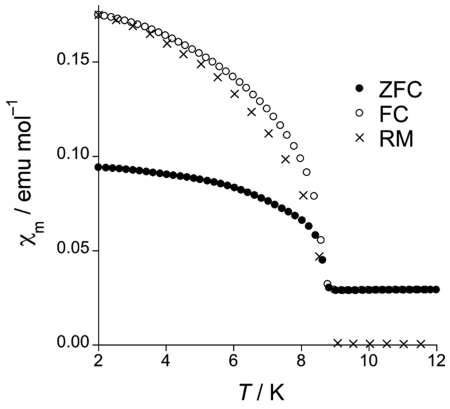

Figure 9. ZFC and FC (applied magnetic field of 25 Oe) and RM for compound **5**, showing the appearance of spontaneous magnetization.

reach 2.1 μ_B, far from the expected 15 μ_B for parallel spin alignment. This behavior is typical of magnets with dominant AF interactions.[52] The hysteresis loop shows a memory effect, with a coercive field of 450 Oe (Figure S4 in the SI).

For compound **6**, χ_m follows an apparently similar trend, reaching a round maximum at 23 K, but no jump is found below the maximum. χ_m keeps decreasing with temperature and only changes the tendency below 10 K, when it increases again (Figure 8). Surprisingly, the ZFC/FC data show an irreversibility above 60 K (Figure 10), associated with a RM that disappears at 66 K, determining the onset of spontaneous magnetization. The ac magnetic susceptibility data show apparently two separated processes, with two maxima in χ', associated with a nonzero signal in χ'' (Figure S5 in the SI). Again, the out-of-phase signal appears to be very weak and noisy. Multiple processes in ac data have been observed in other 2D materials and are related to the low dimensionality of the magnetic networks. The assignment of these two features to multiple phases can be ruled out because of multiple (indirect) experimental evidence. The RM of both features is comparable, both maxima are of the same magnitude, and both appear in the ac and also the ZFC data. Such a major contribution could only arise from major contamination, which cannot exist because these measurements were carried out on grounded hand collected single crystals, avoiding any major contamination.

The field dependence of the magnetization (Figure S6 in the SI) shows a fast increment up to 0.2 T and a linear behavior as

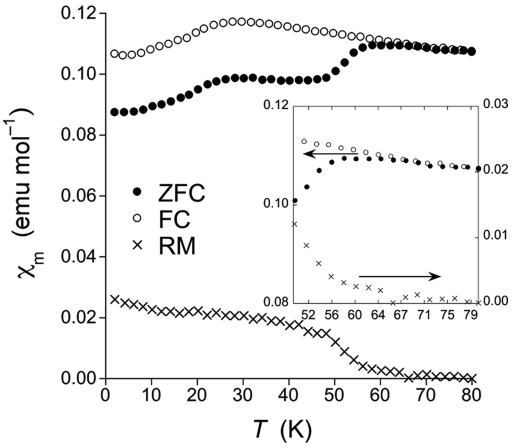

Figure 10. ZFC and FC (applied field of 25 Oe) and RM for compound **6**, showing the appearance of spontaneous magnetization. Inset: Detail of the temperature range where ZFC and FC diverge and when RM disappears.

the magnetic field is further increased. No significant differences were found in the 2−70 K temperature range. M barely reaches 1 μ_B at 7 T and 2 K, far away from the 9 μ_B expected for parallel spin alignment, confirming dominant AF interactions. As the temperature is increased, M shows identical behavior at the low-field range but a higher slope at higher fields to reach higher magnetization values. All of these data confirm again the dominant AF interactions. No hysteresis appears for this compound, which behaves as a very soft magnet.

DISCUSSION

The combination of oxalate, 1,2,4-triazolate, and fluoride anions with divalent first-row metal cations under hydrothermal conditions has demonstrated to be a versatile reaction. The outcome depends on the nature of the transition metal. Using metal oxalates as starting materials, Mn^{2+} only forms one insoluble phase (**5**) that includes all three ligands in its structure. On the other hand, Co^{2+} and Ni^{2+} (**2** and **3**) only yield a completely different phase where the fluoride anion is not incorporated, no matter the reaction conditions. Zn^{2+} reactivity follows this last reaction pattern although it yields a different polymeric arrangement (**4**). Finally, Fe^{2+} shows an intermediate situation. A fluoride-less compound is the main phase (**1**), but a fluoride-containing product is also obtained (**6**), structurally reminiscent of the Mn^{2+} derivative.

It is interesting to note how the growth of phase **1** and that of phase **6** follow opposite building models. **1** is dominated by the coordination mode of the 1,2,4-triazolate units. The 1D triply bridged chains are stabilized by M_2(ox) dimers, whereas the oxalate moieties appear with the classic μ_2-bis-chelating mode. On the contrary, the crystal structure of **6** is dominated by the coordination μ_6 mode of the oxalate dianions, which imposes a planar arrangement of metal centers, with the trz moieties acting as ancillary ligands interconnecting the layers.

The origin for this different behavior should be related to the size of the metal cations. Larger dications, such as Mn^{2+}, can accommodate the μ_6 mode, which requires longer bonding distances. Indeed, **5** includes heptacoordinated metal centers, where the larger atomic radii of Mn^{2+} allows stabilization of μ_3-F bridges. Co^{2+}, Ni^{2+}, and Zn^{2+} are too small to stabilize this multiple bonding, preferring formation of the chain structure.

DOI: 10.1021/ic503032g
Inorg. Chem. 2015, 54, 4678−4687

Fe^{2+} is an intermediate case, where both structural types are stable, even in the absence of the μ_3-F bridges.

This series shows how different structural features result in completely different magnetic behavior. The compounds dominated by the M−trz−M and M−ox−M connectivity (**1**−**3**) exhibit paramagnetic behavior in the entire temperature range studied, with significant AF interactions between spin carriers, stabilizing a nonmagnetic ground state because of the 1D plus dimer magnetic connectivity. In general, AF interactions are significantly stronger through the oxalate bridge.

Compounds **5** and **6** include multiple triangular arrays of antiferromagnetically coupled paramagnetic centers, favoring the appearance of competing interactions. Both materials exhibit spontaneous magnetization and memory effect appearing at 9 and 66 K, respectively, as demonstrated by divergence of the corresponding ZFC/FC data along the RM. No other physical origin can be reasonably claimed for the observed data. Furthermore, the absence of frequency-dependent ac susceptibility suggests that these materials exhibit magnetic ordering. **5** contains μ_3-fluoride and μ_6-oxalate, both of them forming AF triangles. In this case, the Mn−F distances are significantly shorter than the corresponding Mn−oxalate ones, suggesting that the μ_3-fluoride bridge is the major contribution to the magnetic features. On the contrary, the μ_6-oxalate connecting mode in **6** is the only possible origin for competing interactions. Moreover, **6** exhibits the highest T_C reported for oxalate-based magnets (Table 3) and the second highest T_C compared with molecule-based homometallic magnets (Table 4), only surpassed by an oxo-bridged compound.[53]

Table 3. Ordering Temperatures for the Selection of Oxalate-Based Magnets

network	order[a]	T_C (K)	ref
$[Fe^{II}_3(trz)_2(ox)F_2]$ (**6**)	WF	66	this work
$[Fe^{II}Fe^{III}(ox)_3]^-$	ferri	48	54
$[Fe^{II}Fe^{III}(ox)_3]^-$	ferri	45	55
$[Mn^{II}Fe^{III}(ox)_3]^-$	WF	31	56
$[Mn^{II}Fe^{III}(ox)_3]^-$	WF	29	57
$[Mn^{II}Fe^{III}(ox)_3]^-$	WF	27	58
$[Fe^{II}_3(H_2O)_4\{Fe^{III}(ox)_3\}_3]^{3-}$	ferri	26	59
$[Fe(ox)(CH_3OH)]$	WF	23	60
$[Fe^{II}Mn^{III}(ox)_3]^-$	WF	21	61
$[Ni^{II}Mn^{III}(ox)_3]^-$	ferri	21	61
$[Mn^{II}Fe^{III}(ox)_3]^-$	WF	20	62
$[Mn^{II}_3(H_2O)_4\{Fe^{III}(ox)_3\}_3]^{3-}$	WF	14	62
$[NiCr(ox)_3]^-$	ferro	14	63
$[Co^{II}_2(ox)_3]^{2-}$	WF	9	64
$[Mn_3(trz)_2(ox)F_2]$ (**5**)	WF	9	this work
$[MnCr(ox)_3]^-$	ferro	6	63
$[Mn(CH_3OH)Cr(ox)_3]^{2-}$	ferri	5	65

[a]ferro = ferromagnetic; ferri = ferrimagnetic; WF = weak ferromagnet.

CONCLUSIONS

The mixing of two short-pathway connecting organic ligands, oxalate and 1,2,4-triazolate, in the synthesis of coordination polymers has led to the isolation of 3D networks with strong dominant AF superexchange interactions. The geometry of **1**−**3** is dominated by the formation of 1D μ_3-triazole chains interleaved by oxalate-bridged dimers, where the oxalate anion acts in its classic μ_2-bis-chelating coordination mode. The introduction of fluoride anions yields different coordination polymers for the larger metal dications (Mn, **5** and Fe, **6**), whose structure is dominated by the formation of corrugated 2D layers containing μ_6-oxalate connectivity. These are the first compounds where the oxalate ligand connects six paramagnetic centers.

It is worth noting the success of this mixed-ligand homometallic strategy to induce complex magnetic structures. In this case, fluoride anions have allowed, for the first time, the identification of a μ_6-oxalate bridge, a connectivity expected to stabilize magnetic ground states in homometallic compounds because of the appearance of competing interactions. This is confirmed by the spontaneous magnetization observed in both compounds.

6 exhibits the highest ordering temperature for an oxalate-based magnet, when containing Fe^{2+} ($S = 2$). This illustrates the excellent opportunity offered by the μ_6-oxalate arrangement

Table 4. Ordering Temperatures for the Selection of Molecule-Based Weak Ferromagnets

network	linker[a]	S	T_C (K)	ref
$(Et\text{-}NH_3)_2[Fe_2O(ox)_2Cl_2]$	oxo	$^5/_2$	70.0	53
$[Fe_3(trz)_2(ox)F_2]$ (**6**)	oxalate	2	66.0	this work
$Cr(dca)_2$	dca	2	47.0	66
$Co(2\text{-}pymS)_2$	pm	$^3/_2$	42.0	67
$Na_3[Mn_3(HCOO)_9]$	oxo	$^5/_2$	40.0	68
$(NH_4)_2[Fe_2O(ox)_2Cl_2]$	oxo	$^5/_2$	40.0	69
$[NH_2(CH_3)_2]Ni(CHOO)_3$	carboxy	1	35.6	70
$Mn(4\text{-}PMK)(N_3)_2$	azide	$^5/_2$	22.0	71
$Fe[C_6H_5PO_4]$	phos	$^5/_2$	21.5	72
$Mn(2\text{-}pymS)_2$	pm	$^5/_2$	21.2	67
$Ni(mtpo)_2(H_2O)$	pm	1	19.0	73
$Fe_3(imid)_6(imidH)_2$	imidazole	2	17.0	74
$[dmenH][Co_2(HCOO)_6]$	carboxy	$^3/_2$	16.7	75
$Co(N_3)_2(ampyz)$ (3D)	azide	$^3/_2$	16.0	76
$Mn(dca)_2$	dca	$^5/_2$	15.9	77
$Co_2(pmtz)_4$	tetrazole	$^3/_2$	15.0	78
$[NH_2(CH_3)_2]Co(CHOO)_3$	carboxy	$^3/_2$	14.9	75
Co(bIM)(acetate)	imidazole	$^3/_2$	13.0	79
$Mn_2(PMA)(N_3)_4$	azide	$^5/_2$	12.5	80
$Co_4(OMe)_2(O_2CPh)_2(dhq)_2$	alcoxo	$^3/_2$	12.0	81
$Co(N_3)_2(4acpy)_2$	azide	$^3/_2$	11.2	82
$Co(N_3)_2(ampyz)$ (2D)	azide	$^3/_2$	10.0	82
$Co(dca)_2$	dca	$^3/_2$	9.0	83
$[Mn_3(trz)_2(ox)F_2]$ (**5**)	oxalate	$^5/_2$	9.0	this work
$[dmenH][Mn_2(HCOO)_6]$	carboxy	$^5/_2$	8.5	78
$[NH_2(CH_3)_2]Mn(HCOO)_3$	carboxy	$^5/_2$	8.5	73
$Mn(dca)_2(H_2O)$	dca	$^5/_2$	6.3	84
$Co_2(TDDC)_2(H_2O)_2$	carboxy	$^3/_2$	6.0	85
$[Fe(dca)_2]_2(pm)$	dca	2	5.6	86
$Co_4(pico)_4(4,4'\text{-}bpy)_3(H_2O)_2$	carboxy	$^3/_2$	3.0	87
$Co(mtpo)_2(H_2O)$	pm	$^3/_2$	3.0	75
$Mn(btr)_2$	triazole	$^5/_2$	2.6	88

[a]acpy = 4-acetylpyridine; ampyz = 2-aminopyrazine; bIM = benzimidazole; 4,4′-bpy = 4,4′-bipyridyl; carboxy = carboxylate; dca = dicyanamide; dmen = *N*,*N*′-dimethylethylenediamine; Hbtr = 3,4′-bi-1,2,4-triazole; Hmtpo = 5-methyl-1,2,4-triazolo[1,5-*a*]pyrimidin-7(4*H*)-one; phos = phosphate; pico = 3-hydroxypicolinate; pm = pyrimidine; 4-PMK = 4-pyridylmethylketazine; pmtz = 5-(pyrimidyl) tetrazolate; 2-pymSH = 2-mercaptopyrimidine; TDDC = 2,1,3-thiadiazole-4,5-dicarboxylate.

DOI: 10.1021/ic503032g
Inorg. Chem. 2015, 54, 4678−4687

to reach even higher temperature molecule-based magnets. We can envision higher ordering temperatures in μ_6-oxalate magnetic compounds by the incorporation of highly anisotropic metal centers (Co^{2+}) and/or stronger oxalate-based coupling (Ni^{2+}). However, the smaller size of these cations may need larger counteranions to stabilize analogous networks. This work is underway.

■ ASSOCIATED CONTENT

Supporting Information

Additional characterization data, including PXRD and additional magnetic data. The Supporting Information is available free of charge on the ACS Publications website at DOI: 10.1021/ic503032g.

■ AUTHOR INFORMATION

Corresponding Author

*E-mail: jrgalan@iciq.es.

Notes

The authors declare no competing financial interest.

■ ACKNOWLEDGMENTS

We are thankful for the financial support of the EU (ERC Stg Grant 279313, CHEMCOMP), the Spanish Ministerio de Economía y Competitividad (MINECO) through Severo Ochoa Excellence Accreditation 2014−2018 (SEV-2013-0319), and the ICIQ Foundation. M.N.C.-O. gratefully thanks the Marie Curie COFUND Action from the European Commission for cofinancing her postdoctoral fellowship.

■ REFERENCES

(1) Bradshaw, D.; Claridge, J. B.; Cussen, E. J.; Prior, T. J.; Rosseinsky, M. J. *Acc. Chem. Res.* **2005**, *38*, 273−282.
(2) Evangelisti, M.; Luis, F.; de Jongh, L. J.; Affronte, M. *J. Mater. Chem.* **2006**, *16*, 2534−2549.
(3) Coronado, E.; Galán-Mascarós, J. R. *J. Mater. Chem.* **2005**, *15*, 66−74.
(4) Gütlich, P.; Garcia, Y.; Woike, T. *Coord. Chem. Rev.* **2001**, *219*, 839−879.
(5) Mercuri, M. L.; Deplano, P.; Pilia, L.; Serpe, A.; Artizzu, F. *Coord. Chem. Rev.* **2010**, *254*, 1419−1433.
(6) Miller, J. S. *Chem. Soc. Rev.* **2011**, *40*, 3266−3296.
(7) Verdaguer, M.; Bleuzen, A.; Marvaud, V.; Vaissermann, J.; Seuleiman, M.; Desplanches, C.; Scuiller, A.; Train, C.; Garde, R.; Gelly, G.; Lomenech, C.; Rosenman, I.; Veillet, P.; Cartier, C.; Villain, F. *Coord. Chem. Rev.* **1999**, *190−192*, 1023−1047.
(8) Ruiz, E.; Rodríguez-Fortea, A.; Alvarez, S.; Verdaguer, M. *Chem.—Eur. J.* **2005**, *11*, 2135−2144.
(9) Holmes, S. M.; Girolami, G. S. *J. Am. Chem. Soc.* **1999**, *121*, 5593−5594.
(10) Bozdag, K. D.; Yoo, J. W.; Raju, N. P.; McConnell, A. C.; Miller, J. S.; Epstein, A. J. *Phys. Rev. B* **2010**, *82*, 094449.
(11) Coronado, E.; Galán-Mascarós, J. R.; Gómez-García, C. J.; Martínez-Agudo, J. M. *Adv. Mater.* **1999**, *11*, 558−561.
(12) Huang, Z. L.; Drillon, M.; Masciocchi, N.; Sironi, A.; Zhao, J. T.; Rabu, P.; Panissod, P. *Chem. Mater.* **2000**, *12*, 2805−2812.
(13) Rogez, G.; Massobrio, C.; Rabu, P.; Drillon, M. *Chem. Soc. Rev.* **2011**, *40*, 1031−1058.
(14) Miller, J. S.; Manson, J. L. *Acc. Chem. Rev.* **2001**, *34*, 563−570.
(15) Kaneko, W.; Kitagawa, S.; Ohba, M. *J. Am. Chem. Soc.* **2007**, *129*, 248−249.
(16) Sieklucka, B.; Podgajny, R.; Korzeniak, T.; Nowicka, B.; Pinkowicz, D.; Koziel, M. *Eur. J. Inorg. Chem.* **2011**, 305−326.
(17) Her, J. H.; Stephens, P. W.; Kareis, C. M.; Moore, J. G.; Miller, J. S. *Angew. Chem., Int. Ed.* **2010**, *49*, 7773−7775.
(18) Kaye, S. S.; Choi, H. J.; Long, J. R. *J. Am. Chem. Soc.* **2008**, *130*, 16921−16925.
(19) Zheng, Y. Z.; Zheng, Z.; Chen, X. M. *Coord. Chem. Rev.* **2014**, *258*, 1−15.
(20) Gruselle, M.; Train, C.; Boubekeur, K.; Gredin, P.; Ovanesyan, N. *Coord. Chem. Rev.* **2006**, *250*, 2491−2500.
(21) Train, C.; Gheorghe, R.; Krstic, V.; Chamoreau, L. M.; Ovanesyan, N. S.; Rikken, G. L. J. A.; Gruselle, M.; Verdaguer, M. *Nat. Mater.* **2008**, *7*, 729−734.
(22) Coronado, E.; Galán-Mascarós, J. R.; Gómez-García, C. J.; Martínez-Agudo, J. M.; Martínez-Ferrero, E.; Waerenborgh, J. C.; Almeida, M. *J. Solid State Chem.* **2001**, *159*, 391−402.
(23) Hernandez-Molina, M.; Lorenzo-Luis, P. A.; Ruiz-Perez, C. *CrystEngComm* **2001**, *16*, 60−63.
(24) Pardo, E.; Train, C.; Liu, H.; Chamoreau, L. M.; Dhkil, B.; Boubekeur, K.; Lloret, F.; Nakatani, K.; Tokoro, H.; Ohkoshi, S. I.; Verdaguer, M. *Angew. Chem., Int. Ed.* **2012**, *51*, 8356−8360.
(25) Zhang, B.; Zhang, Y.; Wang, Z.; Wang, D.; Baker, P. J.; Pratt, F. L.; Zhu, D. *Sci. Rep.* **2014**, *4*, 6451.
(26) Escuer, A.; Esteban, J.; Perlepes, S. P.; Stamatatos, T. C. *Coord. Chem. Rev.* **2014**, *275*, 87−129.
(27) Ribas, J.; Escuer, A.; Monfort, M.; Vicente, R.; Cortés, R.; Lezama, L.; Rojo, T. *Coord. Chem. Rev.* **1999**, *193−195*, 1027−1068.
(28) Escuer, A.; Aromí, G. *Eur. J. Inorg. Chem.* **2006**, 4721−4736.
(29) Li, R. Y.; Wang, B. W.; Wang, X. Y.; Wang, X. T.; Wang, Z. M.; Gao, S. *Inorg. Chem.* **2009**, *48*, 7174−7180.
(30) Manson, J. L.; Huang, Q. Z.; Lynn, J. W.; Koo, H. J.; Whangbo, M. H.; Bateman, R.; Otsuka, T.; Wada, N.; Argyriou, D. N.; Miller, J. S. *J. Am. Chem. Soc.* **2001**, *123*, 162−172.
(31) Miyasaka, H.; Nakata, K.; Sugiura, K. I.; Yamashita, M.; Clérac, R. *Angew. Chem., Int. Ed.* **2004**, *43*, 707−711.
(32) Miyasaka, H.; Nakata, K.; Lecren, L.; Coulon, C.; Nakazawa, Y.; Fujisaki, T.; Sugiura, K. I.; Yamashita, M.; Clérac, R. *J. Am. Chem. Soc.* **2006**, *128*, 3770−3783.
(33) Manson, J. L.; Schlueter, J. A.; Nygren, C. L. *Dalton Trans.* **2007**, 646−652.
(34) Batten, S. R.; Murray, K. S. *Coord. Chem. Rev.* **2003**, *246*, 103−130.
(35) Clérac, R.; O'Kane, S.; Cowen, J.; Ouyang, X.; Heintz, R.; Zhao, H.; Bazile, M. J.; Dunbar, K. R. *Chem. Mater.* **2003**, *15*, 1840−1850.
(36) Deumal, M.; Rawson, J. M.; Goeta, A. E.; Howard, J. A. K.; Copley, R. C. B.; Robb, M. A.; Novoa, J. J. *Chem.—Eur. J.* **2010**, *16*, 2741−2750.
(37) Fujita, W.; Kikuhi, K. *Chem.—Asian J.* **2009**, *4*, 400−405.
(38) Rabu, P.; Drillon, M. *Adv. Eng. Mater.* **2003**, *5*, 189−210.
(39) Weng, D. F.; Wang, Z. M.; Gao, S. *Chem. Soc. Rev.* **2011**, *40*, 3157−3181.
(40) Ramirez, A. P. *MRS Bull.* **2005**, *30*, 447−451.
(41) Baker, M. L.; Timco, G. A.; Piligkos, S.; Mathieson, J. S.; Mutka, H.; Tuna, F.; Kozłowski, P.; Antkowiak, M.; Guidi, T.; Gupta, T.; Rath, H.; Woolfson, R. J.; Kamieniarz, G.; Pritchard, R. G.; Weihe, H.; Cronin, L.; Rajaraman, G.; Collison, D.; McInnes, E. J. L.; Winpenny, R. E. P. *Proc. Natl. Acad. Sci. U.S.A.* **2012**, *109*, 19113−19118.
(42) Hatnean, J. A.; Raturi, R.; Lefebvre, J.; Leznoff, D. B.; Lawes, G.; Johnson, S. A. *J. Am. Chem. Soc.* **2006**, *128*, 14992−14999.
(43) Wöhlert, S.; Tomkowicz, Z.; Rams, M.; Ebbinghaus, S. G.; Fink, L.; Schmidt, M. U.; Näther, C. *Inorg. Chem.* **2014**, *53*, 8298−8310.
(44) Tsai, J. D.; Yang, C. I. *Dalton Trans.* **2014**, *43*, 15576−15582.
(45) Shores, M. P.; Bartlett, B. M.; Nocera, D. G. *J. Am. Chem. Soc.* **2005**, *127*, 17986−17987.
(46) Burla, M. C.; Caliandro, R.; Camalli, M.; Carrozzini, B.; Cascarano, G. L.; Giacovazzo, C.; Mallamo, M.; Mazzone, A.; Polidori, G.; Spagna, R. *J. Appl. Crystallogr.* **2012**, *45*, 357−361.
(47) Sheldrick, G. M. *Acta Crystallogr.* **2008**, *A64*, 112−122.
(48) Grosjean, A.; Négrier, P.; Bordet, P.; Etrillard, C.; Mondieig, D.; Pechev, S.; Lebraud, E.; Letard, J. F.; Guionneau, P. *Eur. J. Inorg. Chem.* **2013**, 796−802.
(49) Fisher, M. E. *Am. J. Phys.* **1964**, *32*, 343−346.

DOI: 10.1021/ic503032g
Inorg. Chem. 2015, 54, 4678−4687

(50) Meyer, A.; Gleizes, A.; Girerd, J. J.; Verdaguer, M.; Kahn, O. *Inorg. Chem.* **1982**, *21*, 1729−1739.
(51) Glerup, J.; Goodson, P. A.; Hodgson, D. J.; Michelsen, K. *Inorg. Chem.* **1995**, *34*, 6255−6264.
(52) Bellouard, F.; Clemente-Leon, M.; Coronado, E.; Galan-Mascaros, J. R.; Gomez-Garcia, C.; Romero, F. M.; Dunbar, K. R. *Eur. J. Inorg. Chem.* **2002**, 1603−1606.
(53) Armentano, D.; De Munno, G.; Mastropietro, T. F.; Julve, M.; Lloret, F. *J. Am. Chem. Soc.* **2005**, *127*, 10778−10779.
(54) Mathonière, C.; Nuttall, C. J.; Carling, S. G.; Day, P. *Inorg. Chem.* **1996**, *35*, 1201−1206.
(55) Mathonière, C.; Carling, S. G.; Yusheng, D.; Day, P. *J. Chem. Soc., Chem. Commun.* **1994**, 1551−1552.
(56) Clemente-León, M.; Coronado, E.; Gómez-García, C. J.; Soriano-Portillo, A. *Inorg. Chem.* **2006**, *45*, 5653−5660.
(57) Ovanesyan, N. S.; Makhaev, V. D.; Aldoshin, S. M.; Gredin, P.; Boubekeur, K.; Train, C.; Gruselle, M. *Dalton Trans.* **2005**, 3101−3107.
(58) Carling, S. G.; Mathonière, C.; Day, P.; Malik, K. M. A.; Coles, S. J.; Hursthouse, M. B. *J. Chem. Soc., Dalton Trans.* **1996**, 1839−1843.
(59) Coronado, E.; Galán-Mascarós, J. R.; Martí-Gastaldo, C.; Waerenborgh, J. C.; Gaczyński, P. *Inorg. Chem.* **2008**, *47*, 6829−6839.
(60) Zhang, B.; Zhang, Y.; Zhang, J.; Li, J. C.; Zhu, D. *Dalton Trans.* **2008**, 5037−5040.
(61) Coronado, E.; Galán-Mascarós, J. R.; Martí-Gastaldo, C. *J. Mater. Chem.* **2006**, *16*, 2685−2689.
(62) Coronado, E.; Galán-Mascarós, J. R.; Gómez-García, C. J.; Martínez-Ferrero, E.; Almeida, M.; Waerenborgh, J. C. *Eur. J. Inorg. Chem.* **2005**, 2064−2070.
(63) Tamaki, H.; Zhong, Z. J.; Matsumoto, N.; Kida, S.; Koikawa, M.; Achiwa, N.; Hashimoto, Y.; Okawa, H. *J. Am. Chem. Soc.* **1992**, *114*, 6974−6979.
(64) Hernández-Molina, M.; Lloret, F.; Ruiz-Pérez, C.; Julve, M. *Inorg. Chem.* **1998**, *37*, 4131−4135.
(65) Coronado, E.; Galán-Mascarós, J. R.; Martí-Gastaldo, C.; Murcia-Martínez, A. *Dalton Trans.* **2006**, 3294−3299.
(66) Manson, J. L.; Kmety, C. R.; Epstein, A. J.; Miller, J. S. *Inorg. Chem.* **1999**, *38*, 2552−2553.
(67) Zhang, J.; Gao, S.; Zhang, X. X.; Wang, Z. M.; Che, C. M. *Dalton Trans.* **2012**, *41*, 2626−2631.
(68) Paredes-García, V.; Vega, A.; Novak, M. A.; Vaz, M. G. F.; Souza, D. A.; Venegas-Yazigi, D.; Spodine, E. *Inorg. Chem.* **2009**, *48*, 4737−4742.
(69) Armentano, D.; Mastropietro, T. F.; De Munno, G.; Rossi, P.; Lloret, F.; Julve, M. *Inorg. Chem.* **2008**, *47*, 3772−3786.
(70) Wang, X. Y.; Gan, L.; Zhang, S. W.; Gao, S. *Inorg. Chem.* **2004**, *43*, 4615−4625.
(71) Gao, E. Q.; Wang, Z. M.; Yan, C. H. *Chem. Commun.* **2003**, 1748−1749.
(72) Bellito, C.; Federici, F.; Altomare, A.; Rizzi, R.; Ibrahim, S. A. *Inorg. Chem.* **2000**, *39*, 1803−1808.
(73) Lin, Q. P.; Zhang, J.; Cao, X. Y.; Yao, Y. G.; Li, Z. J.; Zhang, L.; Zhou, Z. F. *CrystEngComm* **2010**, *12*, 2938−2942.
(74) Retting, S. J.; Storr, A.; Summers, D. A.; Thompson, R. C.; Trotter, J. *J. Am. Chem. Soc.* **1997**, *119*, 8675−8680.
(75) Wang, Z.; Zhang, X.; Batten, S. R.; Kurmoo, M.; Gao, S. *Inorg. Chem.* **2007**, *46*, 8439−8441.
(76) Boonmak, J.; Nakano, M.; Chaichit, N.; Pakawatchai, C.; Youngme, S. *Inorg. Chem.* **2011**, *50*, 7324−7333.
(77) Manson, J. L.; Kmety, C. R.; Palacio, F.; Epstein, A. J.; Miller, J. S. *Chem. Mater.* **2001**, *13*, 1068−1073.
(78) Rodríguez-Diéguez, A.; Palacios, M. A.; Sironi, A.; Colacio, E. *Dalton Trans.* **2008**, *21*, 2887−2893.
(79) Arai, L.; Nadeem, M. A.; Bhadbhade, M.; Stride, J. A. *Dalton Trans.* **2010**, *39*, 3372−3374.
(80) Gao, E. Q.; Bai, S. Q.; Wang, Z. M.; Yan, C. H. *J. Am. Chem. Soc.* **2003**, *125*, 4984−4985.
(81) Yang, C. I.; Chuang, P. H.; Lee, G. H.; Peng, S. M.; Lu, K. L. *Inorg. Chem.* **2012**, *51*, 757−759.
(82) Wang, X. Y.; Wang, Z. M.; Gao, S. *Inorg. Chem.* **2008**, *47*, 5720−5726.
(83) Jensen, P.; Batten, S. R.; Fallon, G. D.; Moubaraki, B.; Murray, K. S.; Price, D. J. *Chem. Commun.* **1999**, 177−178.
(84) Jensen, P.; Price, D. J.; Batten, S. R.; Moubaraki, B.; Murray, K. S. *Chem.—Eur. J.* **2000**, *6*, 3186−3195.
(85) Li, J. R.; Yu, Q.; Tao, Y.; Bu, X. H.; Ribas, J.; Batten, S. R. *Chem. Commun.* **2007**, 2290−2292.
(86) Takagami, N.; Ishida, T.; Nogami, T. *Bull. Chem. Soc. Jpn.* **2004**, *77*, 1125−1134.
(87) Zeng, M. H.; Zhang, W. X.; Sun, X. Z.; Chen, X. M. *Angew. Chem., Int. Ed.* **2005**, *44*, 3079−3082.
(88) Jia, L. H.; Liu, A. C.; Wang, B. W.; Wang, Z. M.; Gao, S. *Polyhedron* **2011**, *30*, 3112−3115.

DOI: 10.1021/ic503032g
Inorg. Chem. 2015, 54, 4678−4687